Metal-Organic Cages for Molecular Separations

Dawei Zhang, Tanya K. Ronson, You-Quan Zou, Jonathan R. Nitschke*
University of Cambridge, Department of Chemistry, Cambridge, UK, CB2 1EW

ABSTRACT: Separation technology is central to industries as diverse as petroleum, pharmaceuticals, mining, and life sciences. Metal-organic cages, a class of molecular containers formed *via* coordination-driven self-assembly, show great promise as separation agents. Precise control of the shape, size, and functionalization of cage cavities enables them to selectively bind and distinguish a wide scope of physicochemically similar substances in solution. Extensive research has thus been performed involving separations of high value targets with coordination cages, ranging from gases and liquids to compounds dissolved in solution. Enantiopure capsules also show great potential for the separation of chiral molecules. The use of crystalline cages as absorbents, or the incorporation of cages into polymer membranes, could increase the selectivity and efficiency of separation processes. This review covers recent progress in using metal-organic cages to achieve separations, with discussion of the many methods of using them in this context. Challenges and potential future developments are also discussed.

1. Introduction

Since the first extractions of metals from ores and purifications of dyes and medicines from plants, separation techniques have improved the quality of human lives. Seven key separation processes have been identified that,[1] if improved, would reap global benefits. These include the separation of hydrocarbons from crude oil, uranium from seawater, alkenes from alkanes, greenhouse gases from dilute emissions, rare-earth metals from ores, benzene derivatives from each other, and trace contaminants from water. The development of better separation technologies, especially through the discovery of high-performance separation materials that are environmentally benign and low-cost, is thus of vital importance.[2-6]

Metal-organic cages,[7-9] a class of molecular containers[10-16] formed via coordination-driven self-assembly, show great promise as separation agents. They have been widely used for other applications, including molecular recognition,[17-19] chirality sensing,[20,21] stabilization of reactive species,[22,23] and catalysis.[24,25] Owing to the geometries generated by different ligand configurations and metal coordination environments, these assemblies possess immense structural diversity and are often chiral.[26-28] The ability to precisely control the shapes and sizes of their cavities, together with the possibility of inward-facing functionalization, enable them to bind or have the potential to bind all the classes of compounds mentioned in the above key separation processes, indicating great potential for the separation of high value targets.

Compared to metal-organic frameworks (MOFs), a class of solid, porous coordination-based materials that have been widely used for separation,[29-32] an advantage of coordination cages is their tailorable solubilities.[33,34] Cages in solution, in contrast to solid MOFs, can deform or de-ligate so as to encapsulate a guest much larger than the cage pores. Cages can also be incorporated into polymers,[35-38] as fillers, to prepare mixed-matrix membranes for performing separations.[39-42] The solubility of these capsules in different solvents enables them, in contrast to MOFs, to form homogeneous mixtures with polymer matrices, avoiding agglomeration or precipitation of fillers during membrane formation, which may lead to poor separation performance.

This review summarizes recent advances in using metal-organic cages for separations, with emphasis on their multiple modes of use, ranging from cages in solution and in the solid, to polymer membranes and separation columns with cages incorporated.

2. Cages in solution for extraction

Coordination cages have been explored as liquid-phase extractants to extract target molecules from an immiscible liquid phase (liquid-liquid extraction) or a solid phase (solid-liquid extraction). These strategies require binding affinities that are strong enough to pull target molecules from the initial phase into another. Cages bring guests into solvents in which the guests are not normally soluble; the cages are thus useful liquid-phase extractants. Successful application of this extraction strategy requires cages that are stable in different solvents. The high stability of a host-guest complex after extraction can impede extractant recycling and cargo recovery, however stimuli-responsive guest release can be used to overcome these challenges.[43-47]

2.1 Liquid-liquid extraction

The Nitschke group recently reported $Fe^{II}_4L_4$ tetrahedron **1** (Figure 1A), prepared from an azaphosphatrane-based ligand.[48] This cage encapsulates various template anions in water *via* hydrogen bonding and electrostatic interactions. Competitive guest exchange studies indicated a preference for ReO_4^- binding in water over other anions, suggesting the potential of **1** as a perrhenate-selective extractant.

Tetrakis(3,5-bis(trifluoromethyl)phenyl)borate ($BArF^-$) was chosen as the counterion,[49] so that **1** became soluble in the water-immiscible organic solvent, nitromethane. N-butyltrifluoroborate-templated $^nBuBF_3^-\subset$**1** extracted an equimolar amount of ReO_4^- from water into nitromethane; perrhenate displaced the more weakly bound $^nBuBF_3^-$, forming $ReO_4^-\subset$**1**. This extraction proceeded

selectively even in the presence of ten other competing anions. When the solvent was switched from nitromethane to ethyl acetate, the extracted ReO_4^- was released into water as the cage disassembled in ethyl acetate. Evaporation of ethyl acetate, and addition of acetonitrile and $^nBuBF_3^-$, then brought about the regeneration of $^nBuBF_3^-\subset$**1**.

Separation of *para*-dihalogenated benzene derivatives, including *p*-$C_6H_4Cl_2$, *p*-$C_6H_4Br_2$, and *p*-$C_6H_4I_2$, from mixtures of their *ortho*- and *meta*- counterparts was achieved using heterometallic cage **2** featuring two tetra-Rh^{III} metalla-rectangles bridged by two Ag^I centres (Figure 1B).[50] Host-guest studies indicated that only the *para*-dihalobenzenes were encapsulated by cage **2** in methanol, while the other positional isomers were not suitable for its cavity. Crystal structures of the host-guest complexes suggested the selectivity resulted from favourable Ag^I-π interactions and steric effects. Selective extraction of *p*-$C_6H_4Br_2$ from a mixture of dibromobenzenes in *n*-hexane into a methanol solution containing excess **2** was achieved, forming complex *p*-$C_6H_4Br_2\subset$**2**. The extracted *p*-$C_6H_4Br_2$ could be released and recycled *via* precipitation of the Rh^{III} macrocycle under light or upon addition of NaCl, which destroyed the cage. The recovery of **2** occurred upon addition of soluble Ag^I to the methanol solution of the precipitated Rh^{III} macrocycle. This extraction strategy was also used for the efficient separation of *p*-$C_6H_4Cl_2$ or *p*-$C_6H_4I_2$ from the corresponding mixtures of isomers.

The Su group achieved enantioselective separation of atropisomeric molecules, such as 1,1'-bi-2-naphthol (*R*/*S*-BINOL) and *R*/*S*-spirodiol, using enantiopure $Pd_6(RuL_3)_8$ octahedra *Δ*-**3** and *Λ*-**3** (Figure 1C).[51] These two enantiomeric cages were obtained by self-assembly of the corresponding pre-resolved Ru^{II}-based chiral metalloligands and $Pd(BF_4)_2$, and were capable of encapsulating > 10 guests per cage due to the hydrophobic effect. Extraction of these atropisomeric guests from diethyl ether solution (liquid-liquid extraction), or uptake of the guest in solid form (solid-liquid extraction) into an aqueous solution of enantiopure cage, indicated a stereoselectivity of *Δ*-**3** for *R*-isomers and *Λ*-**3** for *S*-isomers.

This separation process thus led to *Δ*-**3** resolving *R*-BINOL with an enantiomeric excess (*ee*) of 34%. Mixing the aqueous host-guest solution with $CHCl_3$ resulted in extraction of the guests into the $CHCl_3$ phase and recovery of the empty cages in the aqueous phase. Further ^1H NMR studies indicated that the resolution process of **3** towards atropisomeric guests was mainly controlled by guest exchange dynamics, in which the inclusion of one guest isomer was more rapid than the other isomer.

Changing the metal of the chiral metalloligand from inert Ru^{II} to the more labile Fe^{II} prevented ligand resolution prior to cage preparation.[52] The Su group instead reported a different method to prepare enantiopure coordination octahedra *Δ*/*Λ*-**4** from racemic Fe^{II}-based metalloligands by

addition of *R*-BINOL during self-assembly. Rapid precipitation of the reaction mixture and slow crystallisation gave rise to metal-organic cages with the opposite handedness. The authors infer this phenomenon to result from distinct kinetic and thermodynamic resolution mechanisms, in which the host-guest complex diastereomer formed through slower crystallisation requires a higher energy barrier to reach this final thermodynamic equilibration. The captured BINOL guests could be liberated from **4** by washing the solid sample several times with diethyl ether. The homochiral **4** thus obtained was used for the enantioseparation of different racemic BINOL derivatives by either liquid-liquid or solid-liquid extraction, giving up to 88% *ee* after two cycles of extraction.

Li *et al*.[53] reported a novel approach for the separation of lanthanide ions based on metal ion self-sorting during cage formation. In a one-pot mixed-metal self-assembly reaction with a 1:1:1 ratio of $Ln_a^{3+}/Ln_b^{3+}/L^1$ in CD_3CN (Figure 1D), narcissistic metal ion self-sorting was observed, exclusively forming homometallic $Ln_4L^1_4$ complexes. For instance, an equimolar mixture of La^{3+}/Lu^{3+} resulted in the exclusive formation of complex $Lu_4L^1_4$ **4**, with La^{3+} ions left in solution. Smaller lanthanides thus incorporated preferentially, and the incorporation of lanthanides having different ionic radii thus appeared to generate strained structures, the avoidance of which led to the observed homometallic selectivity.

The incorporation of hydrophobic di-dodecanamine groups onto the periphery of the ligand (L^2) rendered homometallic $Lu_4L^2_4$ cage **5** soluble in $CHCl_3$, enabling the separation of the two lanthanide ions via extraction of the unreacted La^{3+} from a chloroform phase to a water phase. This strategy was also applicable for the efficient separation of other mixtures of lanthanides, such as La^{3+}/Pr^{3+}, La^{3+}/Eu^{3+}, Pr^{3+}/Eu^{3+}, and Eu^{3+}/Lu^{3+}.

2.2 Solid-liquid extraction

The Jiang group reported a self-assembled carcerand-like cage **6** (Figure 1E),[54] which displayed a temperature-dependent binding preference for C_{60} over C_{70}. The addition of equimolar amounts of C_{60} and C_{70} to **6** in tetrachloroethane resulted in the formation of both $C_{60}\subset$**6** and $C_{70}\subset$**6** at temperatures below 110 °C. However complex $C_{60}\subset$**6** was exclusively formed at 130 °C, leaving C_{70} free in solution. Based on this temperature-dependent fullerene binding preference, a sequential procedure was designed for isolation of individual fullerenes from fullerene soot: (i) simultaneous extraction of C_{60} and C_{70} from solid fullerene soot at 90 °C through formation of their host-guest complexes in solution, (ii) isolation of C_{70} *via* guest displacement by adding additional C_{60} at 130 °C, and (iii) release of C_{60} and recovery of the ligand of the cage by destroying the host-guest complex through addition of 4-dimethylaminopyridine. These procedures enabled the isolation of

C_{60} and C_{70} individually from fullerene soot with purity ≥ 99.5% and the recovery of the ligand of **6** with a yield of 97%.

3. Phase transfer of cages for separation

Phase transfer,[55,56] in which a capsule and its cargo transit from one phase to another across a phase boundary, is a new method of separating capsules together with their guests. After binding a guest in one phase and capsule transition to another, solvent-dependent guest binding behaviour may enable cargo release in the second solvent phase, where host-guest interactions are weaker.[57]

Our initial study showed that three different metal-organic cages and their guests preferentially partitioned into three different phases: water and two mutually immiscible hydrophobic ionic liquids.[58] An anion exchange protocol was then developed to reversibly drive cationic capsules between organic and aqueous phases.[59,60] For both cages **7** and **8** (Figure 2A),[60] their initial SO_4^{2-} counterions rendered the capsules soluble in water. The addition of the hydrophobic anion $B(C_6F_5)_4^-$ to the solution rendered the capsules hydrophobic and causing them to transfer to the upper ethyl acetate (EtOAc) layer.

The phase-transfer sensitivity of each cage to anions was different due to inherent differences in their hydrophobicity, which arose from their charge densities and the hydrophobic surfaces exposed by the subcomponents from which the cages were assembled. When the two cages were dissolved together, sequential phase transfer of the cages was observed upon anion addition. Thus, the transfer of tetrahedron **7** only began after cube **8** had almost completely transferred into EtOAc. This phenomenon led to the separation of two organic cargoes, cyclooctadiene and coronene, which were bound respectively by capsules **7** and **8**, into the two phases (Figure 2A).

Based on a related anion-exchange strategy, we also reported the selective separation of coronene from a mixture of polycyclic aromatic hydrocarbons (PAHs) by phase transfer of coordination cage **9** (Figure 2B).[61] The incorporation of triethylene glycol moieties into its formylpyridine subcomponents improved the solubility and stability of **9** in water when paired with SO_4^{2-} counterions. Tetrahedron **9** was able to selectively encapsulate coronene from a mixture of eight different PAHs in nitromethane and bring it into a new nitromethane phase by transiting through an intermediate water phase, with phase transitioning again being driven by anion metathesis. The bound coronene was released from **9** upon addition of benzene, and both the cage and the purified coronene were recycled *via* further phase separation. Aqueous **9** as the sulfate salt also extracted coronene from a mixture of PAHs in nitromethane, with comparable efficiency to the phase transfer procedure.

This anion exchange concept has been recently applied to three immiscible phases in a circular tube. Circulatory phase transfer of a cage occurred, with the direction of travel depending upon the order of addition of anions.[62] Stimuli that trigger phase transfer of cages without leaving chemical residues were also developed by incorporating longer oligo-ethylene glycol imidazolium chains into coordination cages.[63] These chains responded to temperature, resulting in the cages moving between aqueous and ethylene glycol phases with their cargoes upon heating and cooling. This temperature-responsive behaviour resulted from the expansion or contraction of the oligoethylene glycol imidazolium chains after heating or cooling,[64] which modulated the hydrophobicity and hydrophilicity of the cage.

Grancha *et al*.[65] reported hydroxyl-functionalized $Rh^{II}_{24}L_{24}$ cuboctahedron **10** (Figure 2C) [66] that transfers between phases following pH changes, and thus enables the separation of tetrahydrothiophene and thiophene. More strongly coordinating tetrahydrothiophene bound selectively to the Rh^{II} centres of **10**. The resulting complex transferred to a basic aqueous phase due to deprotonation of **10** and formation of its sodium salt. Separation of the 1-butanol layer enabled the isolation of thiophene. Subsequent ligand exchange at the Rh^{II} sites of **10** with aminopyridine triggered the release of the tetrahydrothiophene cargo, which was extracted into $CHCl_3$. The addition of trifluoroacetic acid to aqueous **10** regenerated the cage in its initial, protonated form and stimulated its transfer into 1-butanol, releasing the aminopyridine into the aqueous layer.

4. Separation through cocrystallisation/precipitation

Isolation of host-guest complexes from a solution containing other competing guests may occur through crystallisation or precipitation. Cocrystallisation of host molecules together with guests has been found to be useful for the enantioselective separation of racemic guests, and it has even worked in cases where no obvious guest binding was observed in solution.[67]

4.1 Enantioseparation through cocrystallisation

In 2010, the Cui group reported the self-assembly of enantiopure M_4L_6 tetrahedron **11** from stereodefined biphenyl bridging ligands and Fe^{III} ions (Figure 3A).[67] The crystal structure of **11** indicated that it was porous, with wide apertures. Although guest binding behaviour was not observed in chloroform, the stereoselective inclusion of 2-butanol or 3-methyl-2-butanol occurred through crystallisation in the presence of the alcohol at room temperature. Three molecules of guest bound per cage, as determined from microanalysis and thermogravimetric analysis. The bound guests could be readily removed from the solid inclusion complex by washing with methanol. The

enantioseparation of these racemic guests was observed with *ee* values of up to 99.5%.

Similarly, the separation of racemic 2-butanol was also achieved using a magnesium-based metallocavitand through a cocrystallisation strategy.[68] Desorption of the included butanol under vacuum indicated an *ee* of 53%.

Prabhakaran *et al*.[69] reported an enantiopure charge-neutral tetrahedron **12** (Figure 3B), which assembled from chiral tris(imido)phosphate trianionic ligands, oxalate, and Pd^{II}. The crystal structure of **12** indicated the presence of large solvent-accessible voids both inside and outside of the cages, resulting in an open 3D-network of diamondoid channels linking the cage internal cavities. Enantiopure **12** separated the enantiomers of chiral epoxides, ketones, and lactones through a cocrystallisation strategy, where these chiral guests were predominantly bound within the external channels. Removal of the guest molecules from the co-crystal by washing with methanol and analysis of the desorbed solution indicated *ee* values of 6-34% for these compounds, with the *R* enantiomers being favoured when using *R*-**12**. The cages could be regenerated either by heating to 100 °C or drying under vacuum overnight followed by recrystallisation from CH_2Cl_2.

By changing the oxalate linkers to chloranilates, enantiomers of new chiral tetrahedron **13** (Figure 3B) with larger cavities were prepared.[70] These cages were also capable of separation of the enantiomers of a series of styrene epoxides *via* cocrystallisation and regenerated *via* the same method used for **12**. An *ee* value of up to 80% was obtained for *R*-4-fluorostyrene oxide using *R*-**13**. The external channels in the crystal again played an important role in separation.

The cocrystallisation strategy for enantioseparation creates chiral spaces comprising both internal cavities and external channels between cages. These hollows interact favourably with specific enantiomers. This approach is similar conceptually with the use of chiral MOFs for enantioselective separations. Many chiral MOFs have been studied as absorbents for enantioseparation, and have even been developed as chiral stationary phases for HPLC and GC,[71-73] or utilized in solid-phase extractions.[74,75] Stereoisomers including amino acids,,[75] amines,[72] alcohols[76] and pharmaceutical molecules[74] have been separated using chiral MOFs. Compared to MOFs, the development of discrete metal-organic cages for chiral separations is still in its infancy and needs further improvement.

4.2 Separation through precipitation

Heteronuclear capsule **14** (Figure 3C), an analogue of **2** (Figure 1B), separated *para*-disubstituted benzene derivatives from regioisomeric mixtures.[77] Capsule **14** bound selectively *para*-xylene and the *para*-dichloro-, *para*-dibromo-, and *para*-diiodo- isomers of benzene, in the

presence of other positional isomers, within its cavity in CD_3OD. The size and shape match, as well as Ag^I-π interactions, were inferred to be the main forces governing molecular recognition.

The addition of diethyl ether to the methanol solution resulted in precipitation of the corresponding host-guest complexes. The encapsulated *para*-xylene was released by washing the precipitate with excess diethyl ether, while the *para*-dihalobenzene molecules were liberated by exposure to light or addition of NaCl to destroy the complexes, as described above, with 91% recovery of the tetra-Rh^{III} metalla-rectangle.

5. Separation using pure solid cages

Solid cages, either in their crystalline or amorphous forms, can be employed directly as absorbents for liquid-solid extractions. The uniform packing between capsules in crystalline solids may lead to regular external channels that may also contribute to target molecule separation, besides their internal cavities. Random cage packing in amorphous solids, in contrast, may result in the adsorption and separation properties being dominated by the internal cage cavities.

5.1 Crystalline cages as absorbents

Chiral crystalline metallomacrocycle **15** (Figure 4A), assembled from four pyridyl-functionalized metallosalen ligands, was reported to separate the enantiomers of racemic alcohols.[78] The stacking of tetrameric **15** resulted in a neutral, porous 3D network. Soaking evacuated crystals in neat racemic 2-butanol at 40 °C for two days led to the selective adsorption of *R*-2-butanol, with one guest molecule bound within the cavity of each tetramer. The *ee* value of the 2-butanol desorbed through distillation was determined to be 99.8%. The resulting solid **15** could be directly recycled and reused for a second cycle of resolution. An alternative approach to recover **15** was to recycle the pyridyl-functionalized metallosalen ligand by addition of dilute HCl, followed by the regeneration of **15** through crystallization. Crystalline **15** also effected the enantioselective separation of 3-methyl-2-butanol in similar fashion, providing the *R*-enantiomer in 99.6% *ee*.

The self-assembly of the same metallosalen ligand with tetrahydrofuran (THF) as a template gave new homochiral metallomacrocycle **16** (Figure 4B),[79] displaying a larger internal cavity. Macrocycle **16** packed into a homochiral porous 3D nanotubular architecture, with six molecules of THF within each of the hexamers in the solid state. Soaking evacuated crystalline **16** in neat racemic 2-pentanol resulted in six equivalents of *R*-2-pentanol being trapped stereoselectively (Figure 4B), which gave rise to an *ee* value of 99.5% after desorption. The resulting solid **16** could be directly

recycled and reused for further resolution, as described in the case of **15**. Similar enantioselective inclusion behaviour was observed for racemic 2-butanol and 3-methyl-2-butanol, favouring the sorption of the *R*-enantiomer in both cases.

A similar pyridyl-functionalized salan ligand and $ZnCl_2$ self-assembled into a homochiral helicate cage, which was able to enantioselectively separate small racemic organic molecules, such as 1-phenylethanol, 1-phenylpropanol, and 1-phenylethylamine, with moderate *ee* values (< 38%), through adsorption in the crystalline state.[80]

Trinuclear cage **17** (Figure 4C) was also capable of separating the enantiomers of 2-butanol,[81] which assembled from two enantiopure [3+3] triphenolic Schiff-base macrocycles and zinc(II). The crystal structure of barrel-shaped **17** revealed a window-to-window arrangement of the two macrocycles, which resulted in the formation of 1D channels. Recrystallisation of **17** in the presence of racemic 2-butanol gave rise to enantioselective binding of *S*-2-butanol inside the channels through coordination to Zn^{II} (Figure 4C), together with additional *S*-2-butanol that occupied the space between cages. The applicability of the cocrystallisation method was limited in this case due to difficulties in growing large crystals. Soaking a dried bulk sample of crystalline **17** into racemic 2-butanol, instead, afforded the low *ee* value of 13% following desorption, which may result from a different packing mode of **17**.

Crystalline cages have also been used for the purification of fullerenes and endohedral metallofullerenes (EMFs). The Ribas group reported tetragonal prismatic metallacage **18** (Figure 5b),[82] assembled from two Zn-porphyrin(tetracarboxylates) and four dinuclear Pd^{II}-linked clips, with $BArF^-$ as the counterions. Cage **18** encapsulated fullerenes of different sizes, including C_{60}, C_{70}, C_{78}, and C_{84}, showing stronger binding affinities for fullerenes larger than C_{60} in a toluene/acetonitrile mixture. Encapsulation of fullerenes also occurred when solid cage **18** soaked in a fullerene-containing toluene solution directly, or by packing solid **18** together with Celite in a short column through which the fullerene-containing solution was eluted. A solvent mixture of 1,2-dichlorobenzene/CS_2 (1/1, v/v) was used to elute this column, enabling recovery of the fullerenes and leaving the empty **18** on the column. Elution of a column containing host-guest complexes of **18** with different fullerenes resulted in initial release of C_{60}, with C_{70} and other higher fullerenes appearing later. This solvent-washing protocol thus enabled the isolation and recovery of 61% of the C_{60} from the fullerene extract.

By changing the metal from Pd^{II} to Cu^{II}, new tetragonal prismatic metallacage **19** (with TfO^- as the counterions) (Figure 5c) with more labile coordination bonds was obtained, resulting in a lower kinetic barrier to fullerene binding and release.[83] Cage **19** displayed preferential binding of C_{70} over C_{60} in solution, while a preference for the smaller C_{60} was observed in the solid state. The different

binding selectivity of **19** in solution and the solid state resulted from higher solid-state rigidity, restricting the internal cavity volume and inducing selectivity for the smaller fullerene.

Mixing crystalline **19** and a toluene solution of Sc_3N-based EMF soot led to the preferential and complete encapsulation of all smaller fullerene species with the exception of $Sc_3N@C_{80}$, rendering $Sc_3N@C_{80}$ the only species left in the supernatant with a purity of 99.5%. Approximately 60% of $Sc_3N@C_{80}$ contained in the initial soot was isolated using this straightforward purification procedure. Moreover, all species bound by solid **19** were liberated through washing with a 1,2-dichlorobenzene/CS_2 (1/1, v/v) solvent mixture, regenerating empty **19**.

The same crystalline cage **19** proved capable of sequential uptake of $U_2@C_{80}$ and $Sc_2CU@C_{80}$ from a toluene solution of Sc/U-based EMF soot, and the encapsulated $U_2@C_{80}$ and $Sc_2CU@C_{80}$ were released from the cavity of **19** using the Ribas group's solvent-washing protocol.[84] Density-functional theory (DFT) calculations hinted that the origins of the high selectivity of **19** in distinguishing the two EMFs derived from their different directional electron-density distributions.

The discovery of stronger binding of C_{78}-EMFs relative to C_{80}-EMFs, resulting from the better shape match of the former, led the same group to investigate the stepwise separation of $U_2@C_{78}$ and $U_2C@C_{78}$ from a toluene solution of a highly complex soot, containing metal adducts of C_{60} to C_{96}, using solid **19**.[85] The selectivity of **19** in distinguishing the two C_{78}-based EMFs again emphasized the essential role played by the electronics of the endohedral clusters in determining the binding strength.

Besides the separation of compounds from solution, the porosity of these crystalline metal-organic cages also renders them promising for gas adsorption after activation. They display a high selectivity towards CO_2 and O_2, indicating their potential in gas separation.[86-88] In common with MOFs, porous crystalline materials have been intensively investigated for these applications. Further improvement will be required before metal-organic cages can match the separation performance or capacity of MOFs, which have been developed for a range of industrially relevant separation processes. These include the removal of acetylene from ethylene,[89,90] paraffin/olefin separation,[91] the removal of H_2O, CO_2, and SO_2 from low-grade natural gas,[92,93] and separation of hexane and xylene isomers.[94-96] MOFs have likewise been employed for the capture of environmentally hazardous gasses from gas mixtures. Examples include capture of toxic gaseous pollutants such as NH_3, H_2S, SO_x, NO_x, CO, and fluorocarbons, and even the capture of warfare agents.[97,98] In addition, they have been employed for separations of H_2/D_2,[99] Xe/Kr,[100] and capture of iodine vapor,[101] which are relevant to nuclear fuel purification and nuclear waste treatment.

5.2 Amorphous cages as absorbents

Amorphous solid $Pd_{12}L_{24}$ capsule **20** (Figure 6A) exhibited excellent dye adsorption and separation ability in water.[102] The amorphous structure of solid **20** was confirmed by an absence of diffraction peaks by PXRD. Solid **20** was able to rapidly and completely adsorb anionic dyes of differing sizes within minutes. Cationic dyes were also adsorbed by **20**, but with much slower uptake rates. Based upon these distinct kinetics, cage **20** removed the anionic dye methyl orange from aqueous solution within 1 min, where it was mixed with cationic dye rhodamine B. This cationic dye was then removed from solution after 120 min by further adsorption. The selectivity of **20** for different dyes resulted from the size of its cavity, its high positive Zeta potential, and the nature of the host-guest interactions involved.

The Jin group prepared metallacycle **21** (Figure 6B).[103] When a solid sample of **21** was respectively treated with the vapour of three hexane isomers, *n*-hexane was captured, whereas the uptake of 2-methylpentane and 2,2-dimethylbutane was very low. The size of the metallacycle, CH···π interactions, and particularly B-H···H-C interactions were inferred to govern the selectivity of hexane recognition. Cycle **21** was also observed to bind with the same selectivity in $CDCl_3$. Suspension of solid **21** in an equimolar mixture of five hexane isomers likewise led to selective *n*-hexane uptake. The extracted *n*-hexane could be released by a vacuum/heating strategy, regenerating empty **21** and enabling it to be recycled.

6. Cage-incorporated materials for separation

Metal-organic cages have been used as fillers, incorporated into polymers to prepare hybrid materials for assisting separation performance.[41] They can be covalently integrated, or freely dispersed, into polymer matrices. A drawback of dispersion is the potential problem of cage leaching. These hybrid materials have been fabricated as membranes for the separation of gases, liquids, or dyes. Coordination cages have been also used to decorate separation columns for chemical analysis, as described below.

6.1 Cage-incorporated polymer membranes

Metal-organic cages have been added to polymers to prepare mixed-matrix membranes.[41] The neat polymer membranes may be permeable to gases, but not selective enough for gas separation.[104,105] When cages are incorporated, the cage pores can provide new pathways for gas diffusion. Cage cavities may provide sorption sites that interact specifically with particular gases,

giving rise to high separation selectivities. However, the stability and compatibility of cages within polymer matrices, and the interactions between cage and matrix should be taken into account, to avoid agglomeration or precipitation of fillers during membrane preparation.

Incorporation of $Cu^{II}_{24}L_{24}$ cuboctahedron **22** bearing triethylene glycol groups (Figure 7A) into cross-linked polyethylene oxide allowed the preparation of membranes for efficient CO_2 separation.[106] The CO_2 and N_2 adsorption isotherms of crystalline **22** alone at 298 K showed a high selectivity for CO_2 over N_2. UV irradiation of the diacrylate and acrylate monomers shown in Figure 7Ab, mixed with cage **22**, enabled fabrication of membranes containing variable concentrations of cage. Homogenous dispersion of **22** into the polymer enhanced CO_2 permeability slightly as compared to the neat polymer membrane. Upon increasing the proportion of **22** in the polymer, the CO_2/N_2 selectivity was seen to steadily increase. The improved gas separation performance of these mixed-matrix membranes was attributed to selective binding of CO_2 to the unsaturated cage Cu^{II} sites.

Analogues of $Cu^{II}_{24}L_{24}$ cuboctahedron **22**,[107] were the only type of cage fillers used in polymer membranes until recently when the incorporation of other coordination cages was reported by the Cook Group.[108] Various $Cu^{II}_{24}L_{24}$ cuboctahedral derivatives, substituted with $-SO_3Na$,[109] long alkyl chains,[110] $-NH_2$,[111] and *tert*-butyl,[112] were incorporated into different polymeric matrices, such as polysulfone, Matrimid® 5218, polyvinylidine fluoride, and poly(1-trimethylsilyl-1)propyne, to gauge their effects upon gas permeability and selectivity. These membranes showed good compatibility between fillers and matrices and were applied to the separation of gas mixtures that included CO_2/CH_4, CO_2/H_2, and CO_2/N_2, with a preference for CO_2 permeance.

These membranes have also been used to separate liquid mixtures by pervaporation.[113,114] For instance, the combination of a $Cu^{II}_{24}L_{24}$ cuboctahedron bearing *tert*-butyl groups and Boltorn W3000,[113] a hyperbranched polymer, enabled the pervaporative separation of toluene from *n*-heptane. Compared with the neat polymer membrane, the transport capacity and selectivity of the hybrid membrane towards aromatic hydrocarbons were significantly improved: both the permeate flux and separation factor increased with increasing cage concentration within a certain range. The enhanced separation performance resulted from the presence of preferential pathways, through the embedded cages, for aromatic molecules, due to their favourable interactions.

In a different strategy to the homogeneous dispersion of coordination cages in polymers described above, Andrés *et al.*[115] reported the deposition of cage-based thin films onto polymer membranes for gas separation. A $Rh^{II}_{24}L_{24}$ cuboctahedron functionalised with pendant aliphatic chains, analogous to $Rh^{II}_{24}L_{24}$ **10** (Figure 2B), assembled at the air-water interface and formed homogenous monolayer films with 2-3 nm thickness through the Langmuir-Blodgett technique.

Deposition of 20-30 monolayers onto the permeable polymer poly(1-trimethylsilyl-1-propyne) allowed the preparation of a cage-based membrane, which showed improved CO_2/N_2 selectivity, compared to the polymer membrane alone, while maintaining the high CO_2 permeance.

The lack of linkage between metal-organic cages and polymers in the examples above may lead to cage leaching. To avoid this issue, Liu *et al.*[116] reported the fabrication of hybrid polymeric membranes with metal-organic cages as nodes, constituting hyper-cross-linked polymer networks for separation applications. The multicomponent condensation reaction of diethylene triamine, tris(2-aminoethyl)amine, and terephthaldehyde, together with zirconium(IV) metal-organic cage **23** (Figure 7B) bearing free amine functionalities, gave an imine-linked polymer membrane with **23** covalently embedded. The cationic nature of **23** led to the strong adsorption of anionic dyes by the hybrid membrane, preventing their passage during filtration. Filtering a mixture of anionic (Brilliant Yellow) and cationic (Rhodamine B) dyes with the cage-embedded membrane thus enabled Rhodamine B alone to pass, resulting in the separation of the two dyes. Moreover, the combination strategy developed here also endowed the mixed-matrix membrane with self-healing abilities, antimicrobial activity, and good mechanical performance.

6.2 Cage-decorated separation columns

Recently metal-organic cages have been used to functionalise chromatographic separation columns. These columns have proven particularly useful for the analytical separation of chiral compounds.

Li *et al.*[117] reported the combination of enantiopure metal-organic cage **17**[81] (Figures 4 and 8) with polymeric ionic liquids to prepare a hybrid material as a chiral stationary phase for capillary electrochromatography (CEC). Polymerization inside of a capillary of imidazolium-based monomers and ethylene glycol dimethacrylates, in the presence of **17**, led to the formation of the monolithic column. The enantiomers of chiral analytes, including mandelic acid, benzoin, and furoin, were efficiently distinguished by this column. The ability of the column to separate positional isomers, such as nitrotoluenes and xylenes, was also strengthened as compared to the same column that did not contain cage **17**. The excellent analytical performance was attributed to the differing molecular interactions between the enantiopure stationary cage with the two enantiomers/isomers of mobile analytes.

Apart from such monolithic columns, packed and open-tubular columns are two other types of columns that have been widely used for CEC. Enantioseparation by CEC was also achieved using open-tubular columns coated with coordination cages.[118] Such columns were prepared by

introducing a cage solution into a pretreated capillary, followed by flushing with N_2 and heating, to form a thin layer of cage on the capillary inner wall. The tubular column coated with **17** was able to separate the enantiomers of chiral amines, alcohols, and ketones, with good repeatability and stability.

Cage **17** was also coated onto the inner wall of capillary columns used for gas chromatography (GC) separations.[119] Mixtures of *n*-alkanes, PAHs, and positional isomers could be separated by this cage-coated capillary column. This method also proved efficient for the separation of racemates, including chiral alcohols, diols, epoxides, ethers, and esters with high enantiomeric differentiation and reproducibility. The cages were able, thus, to interact differentially with different analytes, giving rise to different retention times on the column.

7. Conclusions and perspective

Although metal-organic cages have been used for many separations, the cages thus employed represent only a small proportion of the large number of cages that have been reported capable of selective guest recognition.[17-19] Almost all of the examples discussed in this review are fundamental proof-of-concept studies. In order to extend the use of metal-organic cages to real industrial processes, consideration of the scale-up of separation processes and the recovery of the cages in larger scale separation scenarios will be crucial, building upon the methods that have already been developed at the laboratory scale. Broader consideration of the stability, toxicity and potential environmental harm, as well as the cost of materials, will be crucial in order to assess the feasibility of the use of these materials in industry.

An advantage of using dissolved cages is the enhanced dynamic character in solution as opposed to the solid state, which can allow partial opening to permit binding of guests larger than the size of cage portals. Apart from the shapes, sizes, and functionalities of cage cavities, strategies are needed to engineer the pores of crystalline cage absorbents.[120,121] Cages incorporated into polymers have successfully facilitated cargo separation and show promise for practical use in industry, provided cages do not leach. The use of embedded metal-organic cages as crosslinks directly connecting polymer chains can avoid this problem. Lastly, coordination cages that are permanently porous ionic liquids have recently been reported.[122] These cage materials are both porous and fluid,[122-126] and are capable of binding guests including ozone-depleting chlorofluorocarbons,[122] providing a promising class of materials for future chemical separations. The versatile use of metal-organic cages and their high guest binding selectivities will enable them to be integrated into current separation technologies, and ultimately address challenging separations of great industrial relevance.

Acknowledgements

This work was supported by the European Research Council (695009) and the UK Engineering and Physical Sciences Research Council (EPSRC EP/P027067/1). D. Z. acknowledges a Herchel Smith Research Fellowship from the University of Cambridge.

Author contributions

D.Z. and T.K.R. researched the literature for the review. D.Z. wrote the first version of the manuscript. T.K.R., Y.Q.Z. and D.Z. prepared the figures. All authors contributed to the discussion and editing of the manuscript before submission.

Competing interests

The authors declare no competing interests.

Figures and captions

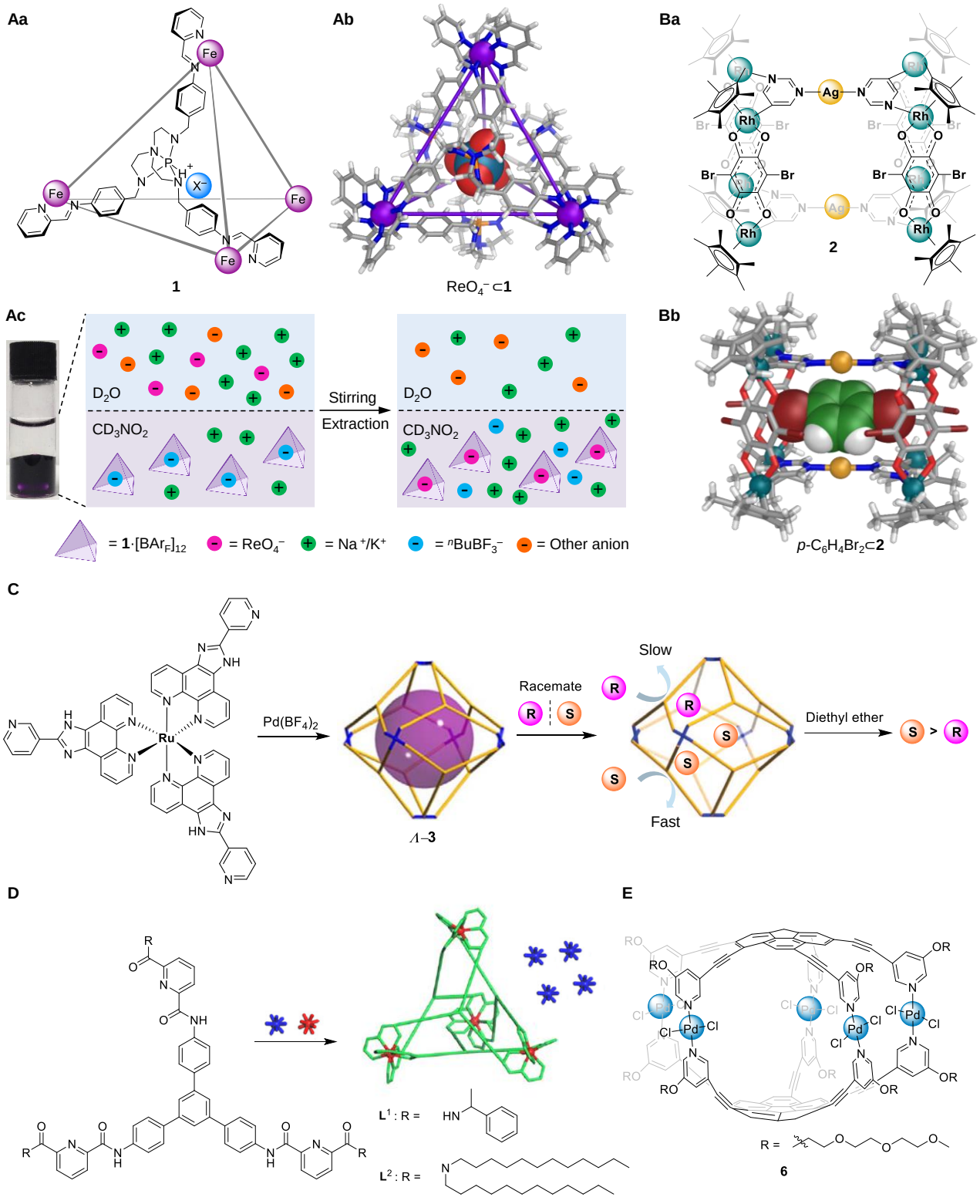

Figure 1 | Metal-organic cages used for cargo extraction in solution. A | Schematic structure of **1** (**Aa**), X-ray crystal structure of ReO_4^-⊂**1** (**Ab**), and selective liquid-liquid extraction of ReO_4^- by **1** (**Ac**), in the presence of other competing anions.[49] **B |** Schematic structure of **2** (**Ba**) and X-ray crystal structure of *p*-$C_6H_4Br_2$⊂**2** (**Bb**).[50] **C |** Self-assembly of *Λ*-**3** and the proposed resolution process, relying on exchange dynamics of the guest atropisomers with *Λ*-**3**, in which the inclusion of the *S*-isomer was more rapid than the *R*-isomer.[51] **D |** Metal ion self-sorting behaviour in the self-assembly of $Ln_4L^1_4$ **4** and $Ln_4L^2_4$ **5**.[53] **E |** Structure of **6**.[54]

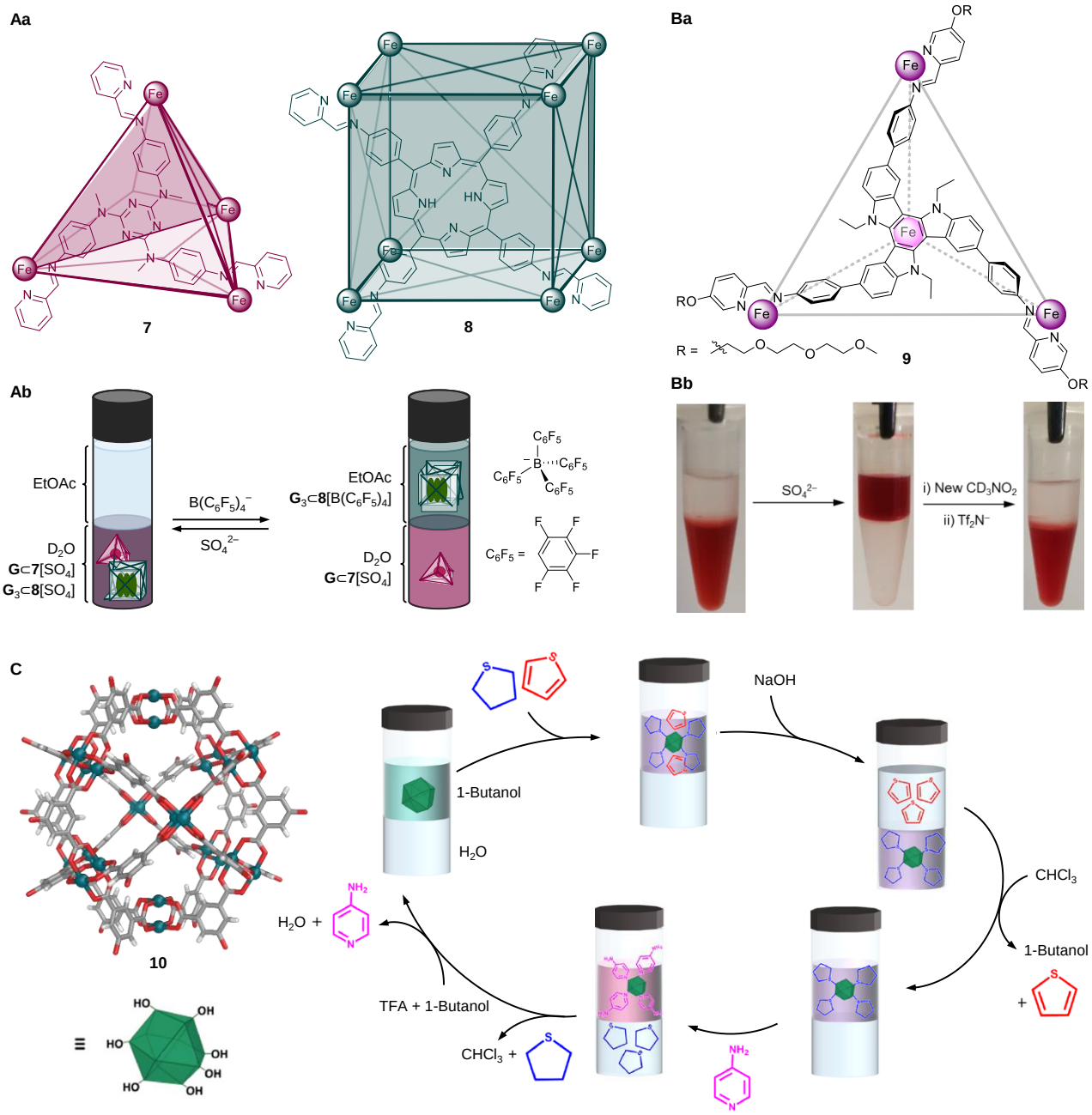

Figure 2 | Phase transfer of metal-organic cages for target separation. A | Schematic structures of **7** and **8** (**Aa**) and separation of the two cargoes, cyclooctadiene and coronene, which were bound by **7** and **8** respectively, by preferential phase transfer of **8** (**Ab**).[60] **B |** Schematic structure of **9** (**Ba**) and photographs of sequential phase transfer of **9** from a CD_3NO_2 layer (lower) to a new CD_3NO_2 layer through an intermediate D_2O phase (upper) (**Bb**).[61] **C |** Crystal structure of **10**[66] and scheme illustrating the separation of thiophene and tetrahydrothiophene by phase transfer of **10**.[65]

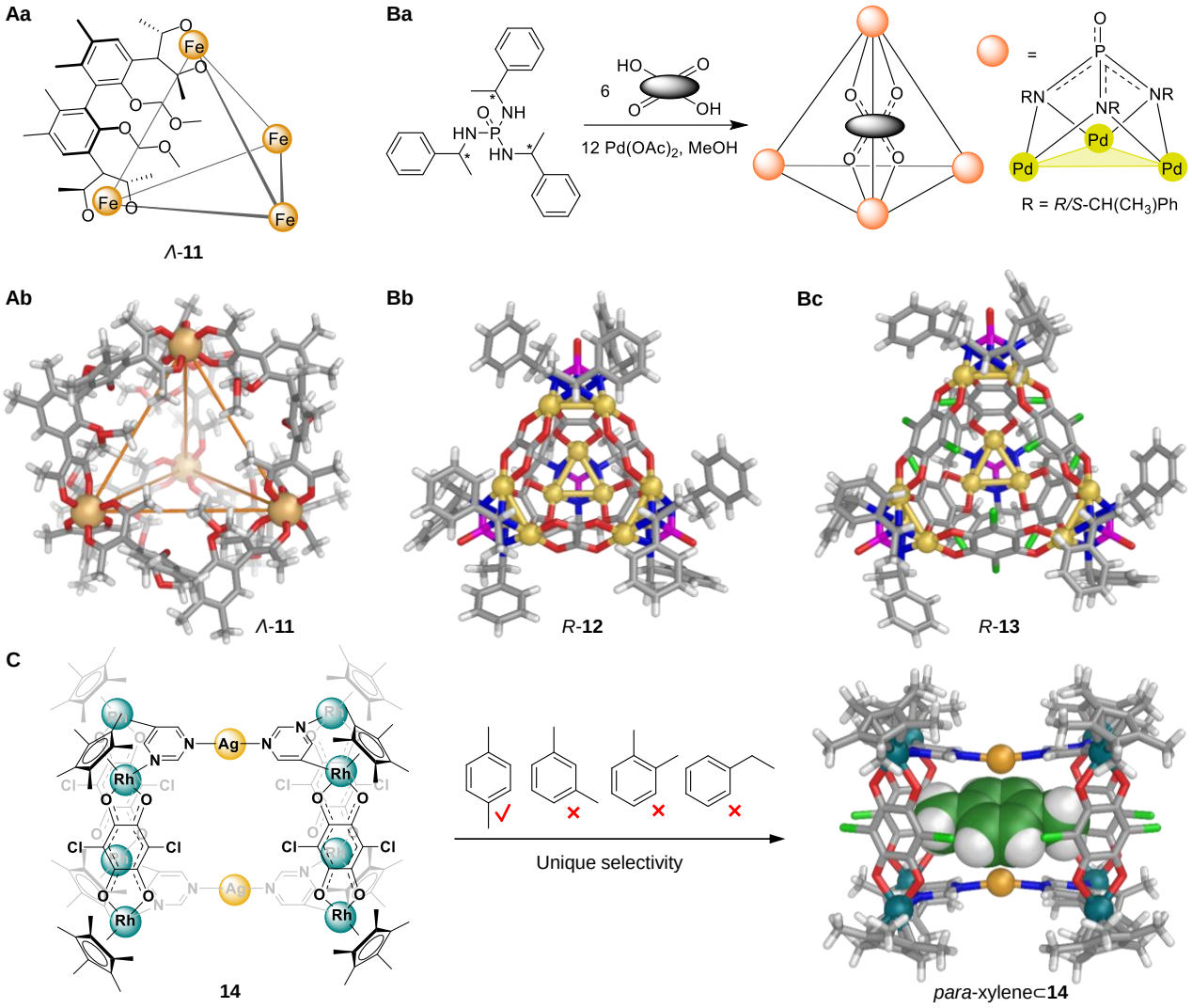

Figure 3 | Metal-organic cages for guest separation through crystallisation or precipitation. A | Schematic structure (**Aa**) and crystal structure (**Ab**) of homochiral *Λ*-**11**.[67] **B |** Self-assembly of enantiopure **12** and **13** (**Ba**), and crystal structures of *R*-**12** (**Bb**) and *R*-**13** (**Bc**).[69,70] **C |** Schematic structure of **14** and crystal structure of *para*-xylene⊂**14**, highlighting the unique guest binding selectivity.[77]

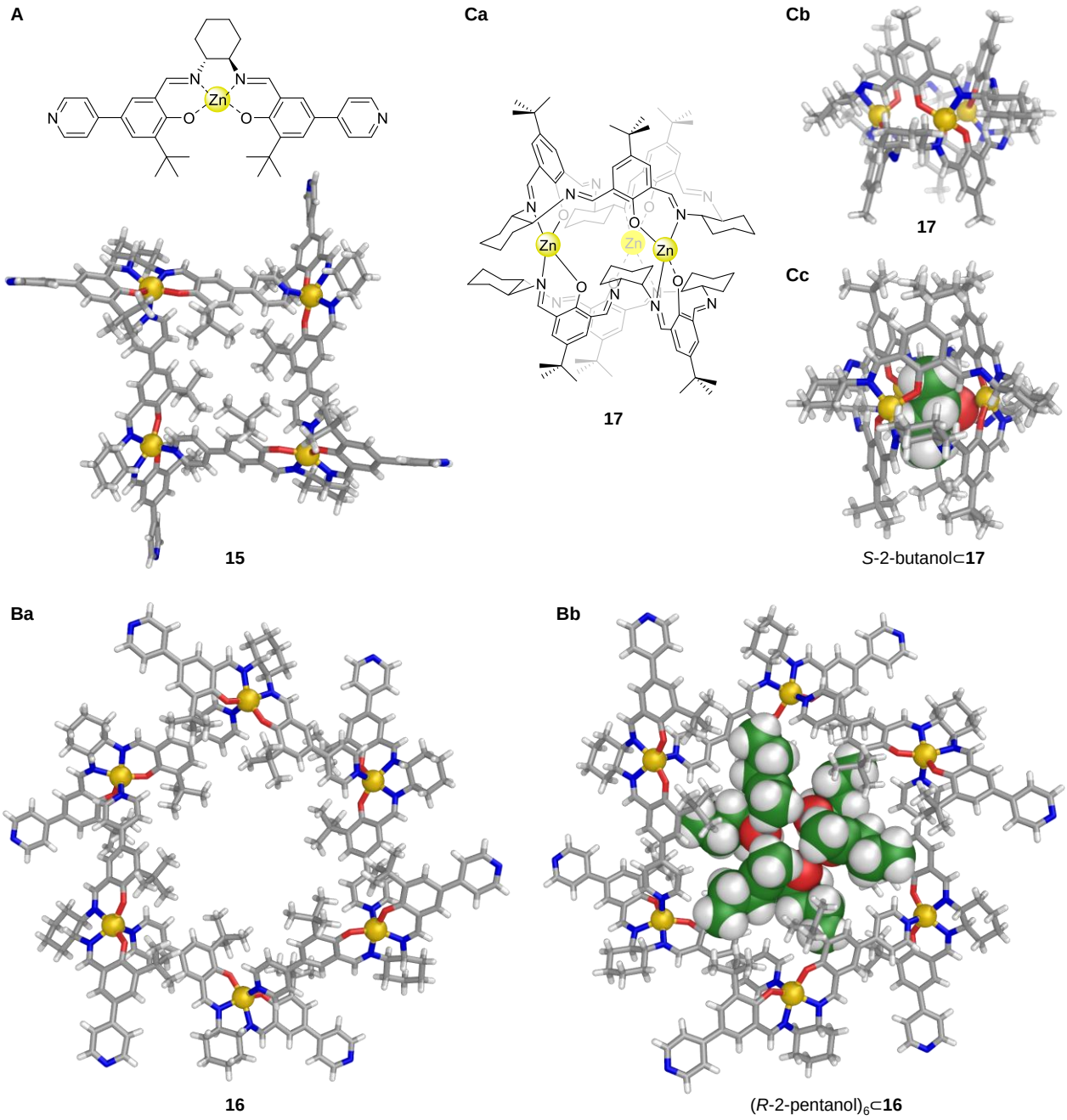

Figure 4 | Crystalline metal-organic cages as absorbents for target separation. A | Schematic structure of the monomeric unit and crystal structure of tetramer **15**.[78] **B |** Crystal structures of hexamer **16** (**Ba**) and (*R*-2-pentanol)$_6$⊂**16** (**Bb**).[79] **C |** Schematic structure of **17** (**Ca**), and crystal structures of **17** (**Cb**) and *S*-2-butanol⊂**17** (**Cc**).[81]

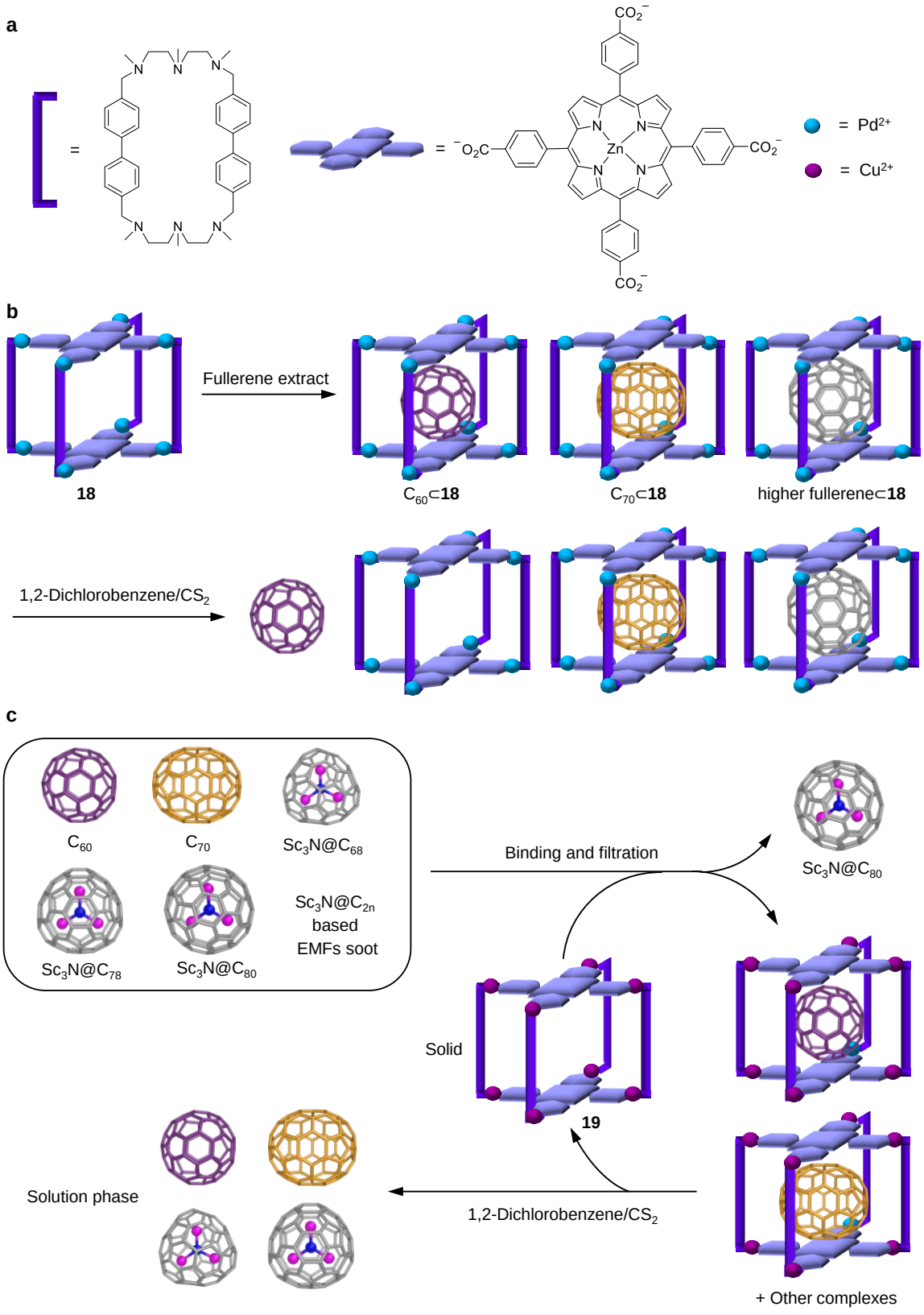

Figure 5 | Crystalline metal-organic cages for fullerene separation. a | Schemes illustrating the compositions of the capsules.[82,83] **b |** The encapsulation of various fullerenes from a fullerene extract with **18** and the selective release of C_{60} by washing with a 1,2-dichlorobenzene/CS_2 (1/1, v/v).[82] **c |** The encapsulation of various fullerene species within crystalline **19** from a Sc_3N-based EMF soot, with the exception of binding $Sc_3N@C_{80}$, which was left in solution. Filtering the sample led to the separation of $Sc_3N@C_{80}$ from other solid host-guest complexes, and **19** could be recycled by washing with 1,2-dichlorobenzene/CS_2 (1/1, v/v).[83]

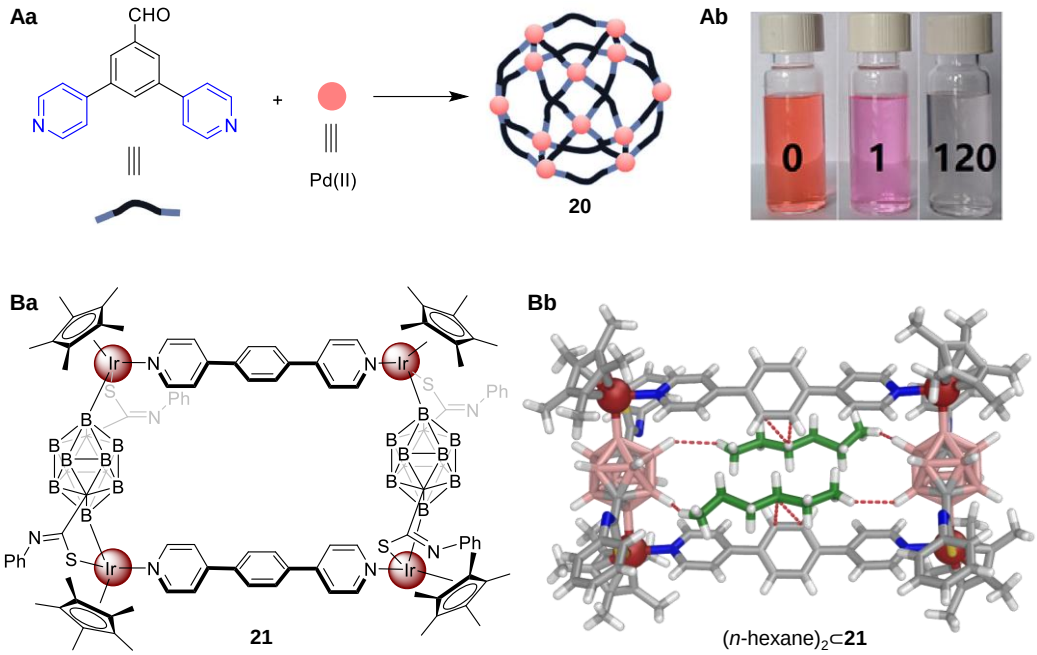

Figure 6 | Amorphous metal-organic cages as absorbents for guest separation. A | Self-assembly of **20** (**Aa**) and photographs showing the time-dependent, stepwise adsorption behaviour of **20** for a mixture of cationic (rhodamine B) and anionic (methyl orange) dyes in water (**Ab**). After 1 min of adsorption, the initial red orange solution became pink, corresponding to the colour of the cationic dye. Adsorption for 120 minutes enabled the complete removal of the remaining cationic dye.[102] **B |** Schematic structure of **21** (**Ba**) and crystal structure of (*n*-hexane)$_2$⊂**21** (**Bb**).[103]

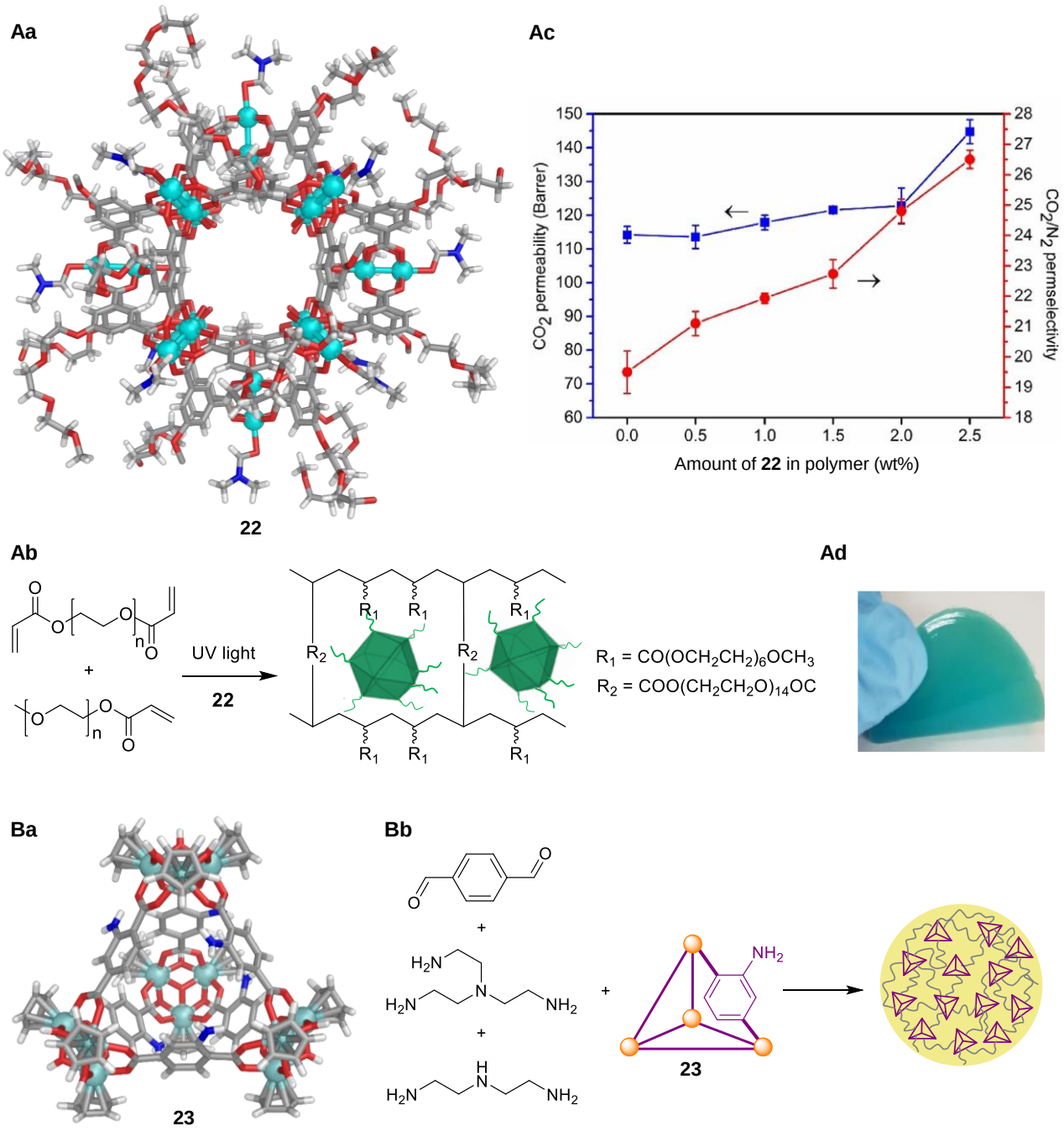

Figure 7 | Metal-organic cage incorporated polymer membranes for target separation. A | Crystal structure of **22** (**Aa**), UV polymerization of diacrylate and acrylate monomers in the presence of **22** (**Ab**), CO_2 permeability and CO_2/N_2 permselectivity of the membrane containing different amounts of **22** (**Ac**), and a photograph of the cage-incorporated membrane (**Ad**).[106] **B |** Crystal structure of **23** (**Ba**) and formation of the hybrid membrane with **23** covalently embedded *via* imine linkages (**Bb**).[116]

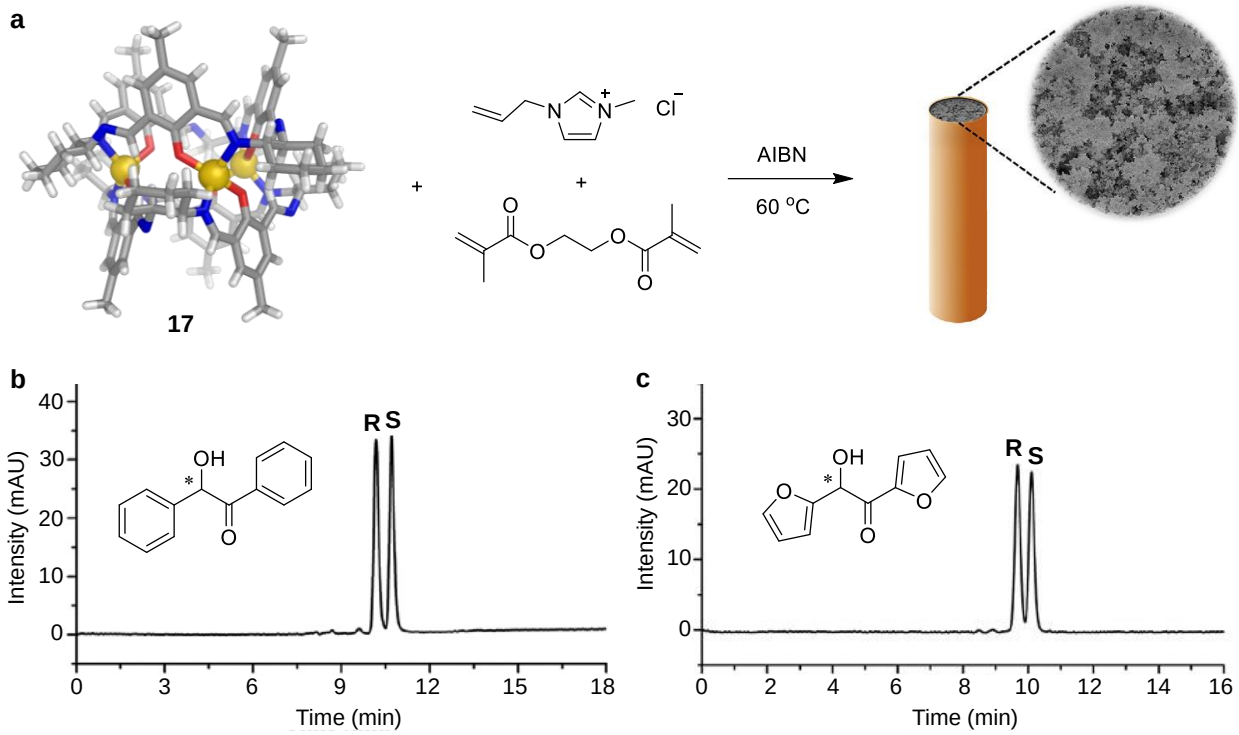

Figure 8 | Metal-organic cage decorated CEC column for target separation. a | Preparation of a poly(ionic liquid)-based monolithic column with **17** embedded.[117] **b** and **c |** Separation performances of racemic benzoin (**b**) and furoin (**c**) with the cage-decorated CEC column.

References

1 Sholl, D. S. & Lively, R. P. Seven chemical separations to change the world. *Nature* **532**, 435-437 (2016).

2 Park, H. B. *et al.* Polymers with cavities tuned for fast selective transport of small molecules and ions. *Science* **318**, 254-258 (2007).

3 McKeown, N. B. & Budd, P. M. Polymers of intrinsic microporosity (PIMs): organic materials for membrane separations, heterogeneous catalysis and hydrogen storage. *Chem. Soc. Rev.* **35**, 675-683 (2006).

4 Jie, K., Zhou, Y., Li, E. & Huang, F. Nonporous adaptive crystals of pillararenes. *Acc. Chem. Res.* **51**, 2064-2072 (2018).

5 Surwade, S. P. *et al.* Water desalination using nanoporous single-layer graphene. *Nat. Nanotechnol.* **10**, 459-464 (2015).

6 Davis, M. E. Ordered porous materials for emerging applications. *Nature* **417**, 813-821 (2002).

7 Zhang, D., Ronson, T. K. & Nitschke, J. R. Functional capsules via subcomponent self-assembly. *Acc. Chem. Res.* **51**, 2423-2436 (2018).

8 Cook, T. R. & Stang, P. J. Recent developments in the preparation and chemistry of metallacycles and metallacages via coordination. *Chem. Rev.* **115**, 7001-7045 (2015).

9 Han, M., Engelhard, D. M. & Clever, G. H. Self-assembled coordination cages based on banana-shaped ligands. *Chem. Soc. Rev.* **43**, 1848-1860 (2014).

10 Little, M. A. & Cooper, A. I. The chemistry of porous organic molecular materials. *Adv. Funct. Mater.* (2020).

11 Brotin, T. & Dutasta, J. P. Cryptophanes and their complexes-present and future. *Chem. Rev.* **109**, 88-130 (2009).

12 Isaacs, L. Stimuli responsive systems constructed using cucurbit[n]uril-type molecular containers. *Acc. Chem. Res.* **47**, 2052-2062 (2014).

13 Zhang, M., Yan, X., Huang, F., Niu, Z. & Gibson, H. W. Stimuli-responsive host-guest systems based on the recognition of cryptands by organic guests. *Acc. Chem. Res.* **47**, 1995-2005 (2014).

14 Qi, Z. & Schalley, C. A. Exploring macrocycles in functional supramolecular gels: from stimuli responsiveness to systems chemistry. *Acc. Chem. Res.* **47**, 2222-2233 (2014).

15 Peng, S. *et al.* Strapped calix[4]pyrroles: from syntheses to applications. *Chem. Soc. Rev.* **49**, 865-907 (2020).

16 Mastalerz, M. Porous shape-persistent organic cage compounds of different size, geometry, and function. *Acc. Chem. Res.* **51**, 2411-2422 (2018).

17 Ward, M. D., Hunter, C. A. & Williams, N. H. Coordination cages based on bis(pyrazolylpyridine) ligands: structures, dynamic behavior, guest binding, and catalysis. *Acc. Chem. Res.* **51**, 2073-2082 (2018).

18 Custelcean, R. Anion encapsulation and dynamics in self-assembled coordination cages. *Chem. Soc. Rev.* **43**, 1813-1824 (2014).

19 Ballester, P. Anion binding in covalent and self-assembled molecular capsules. *Chem. Soc. Rev.* **39**, 3810-3830 (2010).

20 Hembury, G. A., Borovkov, V. V. & Inoue, Y. Chirality-sensing supramolecular systems. *Chem. Rev.* **108**, 1-73 (2008).

21 Young, M. C., Holloway, L. R., Johnson, A. M. & Hooley, R. J. A supramolecular sorting hat: stereocontrol in metal-ligand self-assembly by complementary hydrogen bonding. *Angew. Chem. Int. Ed.* **53**, 9832-9836 (2014).

22 Galan, A. & Ballester, P. Stabilization of reactive species by supramolecular encapsulation. *Chem. Soc. Rev.* **45**, 1720-1737 (2016).

23 Yamashina, M., Sei, Y., Akita, M. & Yoshizawa, M. Safe storage of radical initiators within a polyaromatic nanocapsule. *Nat. Commun.* **5**, 4662 (2014).

24 Brown, C. J., Toste, F. D., Bergman, R. G. & Raymond, K. N. Supramolecular catalysis in metal-ligand cluster hosts. *Chem. Rev.* **115**, 3012-3035 (2015).

25 Grommet, A. B., Feller, M. & Klajn, R. Chemical reactivity under nanoconfinement. *Nat. Nanotechnol.* **15**, 256-271 (2020).

26 Chen, L. J., Yang, H. B. & Shionoya, M. Chiral metallosupramolecular architectures. *Chem. Soc. Rev.* **46**, 2555-2576 (2017).

27 Pullen, S. & Clever, G. H. Mixed-ligand metal-organic frameworks and heteroleptic coordination cages as multifunctional scaffolds-a comparison. *Acc. Chem. Res.* **51**, 3052-3064 (2018).

28 De, S., Mahata, K. & Schmittel, M. Metal-coordination-driven dynamic heteroleptic architectures. *Chem. Soc. Rev.* **39**, 1555-1575 (2010).

29 Li, J. R., Sculley, J. & Zhou, H. C. Metal-organic frameworks for separations. *Chem. Rev.* **112**, 869-932 (2012).

30 Rojas, S. & Horcajada, P. Metal-organic frameworks for the removal of emerging organic contaminants in water. *Chem. Rev.* (2020).

31 Zhao, X., Wang, Y., Li, D. S., Bu, X. & Feng, P. Metal-organic frameworks for separation. *Adv. Mater.* **30**, e1705189 (2018).

32 Adil, K. *et al.* Gas/vapour separation using ultra-microporous metal-organic frameworks: insights into the structure/separation relationship. *Chem. Soc. Rev.* **46**, 3402-3430 (2017).

33 Percastegui, E. G., Mosquera, J. & Nitschke, J. R. Anion exchange renders hydrophobic capsules and cargoes water-soluble. *Angew. Chem. Int. Ed.* **56**, 9136-9140 (2017).

34 Cook, T. R., Zheng, Y. R. & Stang, P. J. Metal-organic frameworks and self-assembled supramolecular coordination complexes: comparing and contrasting the design, synthesis, and functionality of metal-organic materials. *Chem. Rev.* **113**, 734-777 (2013).

35 Gu, Y. *et al.* Photoswitching topology in polymer networks with metal–organic cages as crosslinks. *Nature* **560**, 65-69 (2018).

36 Zhukhovitskiy, A. V. *et al.* Highly branched and loop-rich gels via formation of metal–organic cages linked by polymers. *Nat. Chem.* **8**, 33-41 (2016).

37 Hosono, N. & Kitagawa, S. Modular design of porous soft materials via self-organization of metal-organic cages. *Acc. Chem. Res.* **51**, 2437-2446 (2018).

38 Foster, J. A. *et al.* Differentially addressable cavities within metal-organic cage-cross-linked polymeric hydrogels. *J. Am. Chem. Soc.* **137**, 9722-9729 (2015).

39 Koros, W. J. & Zhang, C. Materials for next-generation molecularly selective synthetic membranes. *Nat. Mater.* **16**, 289-297 (2017).

40 Liu, G., Jin, W. & Xu, N. Two-dimensional-material membranes: a new family of high-performance separation membranes. *Angew. Chem. Int. Ed.* **55**, 13384-13397 (2016).

41 Dechnik, J., Gascon, J., Doonan, C. J., Janiak, C. & Sumby, C. J. Mixed-matrix membranes. *Angew. Chem. Int. Ed.* **56**, 9292-9310 (2017).

42 Bastani, D., Esmaeili, N. & Asadollahi, M. Polymeric mixed matrix membranes containing zeolites as a filler for gas separation applications: A review. *J. Ind. Eng. Chem.* **19**, 375-393 (2013).

43 Han, M. *et al.* Light-triggered guest uptake and release by a photochromic coordination cage. *Angew. Chem. Int. Ed.* **52**, 1319-1323 (2013).

44 Kim, T. Y., Vasdev, R. A. S., Preston, D. & Crowley, J. D. Strategies for reversible guest uptake and release from metallosupramolecular architectures. *Chem. Eur. J.* **24**, 14878-14890 (2018).

45 Cullen, W., Turega, S., Hunter, C. A. & Ward, M. D. pH-dependent binding of guests in the cavity of a polyhedral coordination cage: reversible uptake and release of drug molecules. *Chem. Sci.* **6**, 625-631 (2015).

46 Kishi, N. *et al.* Facile catch and release of fullerenes using a photoresponsive molecular tube. *J. Am. Chem. Soc.* **135**, 12976-12979 (2013).

47 Chan, A. K., Lam, W. H., Tanaka, Y., Wong, K. M. & Yam, V. W. Multiaddressable molecular rectangles with reversible host-guest interactions: modulation of pH-controlled guest release and capture. *Proc. Natl. Acad. Sci. U. S. A.* **112**, 690-695 (2015).

48 Zhang, D. *et al.* Anion binding in water drives structural adaptation in an azaphosphatrane-functionalized $Fe^{II}{}_4L_4$ tetrahedron. *J. Am. Chem. Soc.* **139**, 6574-6577 (2017).

49 Zhang, D., Ronson, T. K., Mosquera, J., Martinez, A. & Nitschke, J. R. Selective anion extraction and recovery using a $Fe^{II}{}_4L_4$ cage. *Angew. Chem. Int. Ed.* **57**, 3717-3721 (2018).

50 Zhang, H. N., Lu, Y., Gao, W. X., Lin, Y. J. & Jin, G. X. Selective encapsulation and separation of dihalobenzene isomers with discrete heterometallic macrocages. *Chem. Eur. J.* **24**, 18913-18921 (2018).

51 Wu, K. *et al.* Homochiral D_4-symmetric metal-organic cages from stereogenic Ru(II) metalloligands for effective enantioseparation of atropisomeric molecules. *Nat. Commun.* **7**, 10487 (2016).

52 Hou, Y. J. *et al.* Design and enantioresolution of homochiral Fe(II)-Pd(II) coordination cages from stereolabile metalloligands: stereochemical stability and enantioselective separation. *J Am. Chem. Soc.* **140**, 18183-18191 (2018).

53 Li, X.-Z. *et al.* A supramolecular lanthanide separation approach based on multivalent cooperative enhancement of metal ion selectivity. *Nat. Commun.* **9**, 547 (2018).

54 Sun, W. *et al.* Self-assembled carcerand-like cage with a thermoregulated selective binding preference for purification of high-purity C_{60} and C_{70}. *J. Org. Chem.* **83**, 14667-14675 (2018).

55 Wei, G. T., Yang, Z., Lee, C. Y., Yang, H. Y. & Wang, C. R. Aqueous-organic phase transfer of gold nanoparticles and gold nanorods using an ionic liquid. *J. Am. Chem. Soc.* **126**, 5036-5037 (2004).

56 Yuan, X. *et al.* Synthesis of highly fluorescent metal (Ag, Au, Pt, and Cu) nanoclusters by electrostatically induced reversible phase transfer. *ACS Nano* **5**, 8800-8808 (2011).

57 Bolliger, J. L., Ronson, T. K., Ogawa, M. & Nitschke, J. R. Solvent effects upon guest binding and dynamics of a $Fe^{II}{}_4L_4$ cage. *J. Am. Chem. Soc.* **136**, 14545-14553 (2014).

58 Grommet, A. B., Bolliger, J. L., Browne, C. & Nitschke, J. R. A triphasic sorting system: coordination cages in ionic liquids. *Angew. Chem. Int. Ed.* **54**, 15100-15104 (2015).

59 Grommet, A. B. & Nitschke, J. R. Directed phase transfer of an $Fe^{II}{}_4L_4$ cage and encapsulated cargo. *J. Am. Chem. Soc.* **139**, 2176-2179 (2017).

60 Grommet, A. B. *et al.* Anion exchange drives reversible phase transfer of coordination cages and their cargoes. *J. Am. Chem. Soc.* **140**, 14770-14776 (2018).

61 Zhang, D., Ronson, T. K., Lavendomme, R. & Nitschke, J. R. Selective separation of polyaromatic hydrocarbons by phase transfer of coordination cages. *J. Am. Chem. Soc.* **141**, 18949-18953 (2019).

62 Mihara, N., Ronson, T. K. & Nitschke, J. R. Different modes of anion response cause circulatory phase transfer of a coordination cage with controlled directionality. *Angew. Chem. Int. Ed.* **58**, 12497-12501 (2019).

63 Nguyen, B. T., Grommet, A. B., Tron, A., Georges, M. C. A. & Nitschke, J. R. Heat engine drives transport of an $Fe^{II}_4L_4$ cage and cargo. *Adv. Mater.*, e1907241 (2020).

64 Yao, W. *et al.* Tuning the hydrophilicity and hydrophobicity of the respective cation and anion: reversible phase transfer of ionic liquids. *Angew. Chem. Int. Ed.* **55**, 7934-7938 (2016).

65 Grancha, T. *et al.* Phase transfer of rhodium(II)-based metal-organic polyhedra bearing coordinatively bound cargo enables molecular separation. *J. Am. Chem. Soc.* **141**, 18349-18355 (2019).

66 Carne-Sanchez, A. *et al.* Postsynthetic covalent and coordination functionalization of rhodium(II)-based metal-organic polyhedra. *J. Am. Chem. Soc.* **141**, 4094-4102 (2019).

67 Liu, T., Liu, Y., Xuan, W. & Cui, Y. Chiral nanoscale metal-organic tetrahedral cages: diastereoselective self-assembly and enantioselective separation. *Angew. Chem. Int. Ed.* **49**, 4121-4124 (2010).

68 Li, Y. *et al.* Bulky metallocavitands with a chiral cavity constructed by aluminum and magnesium atrane-likes: enantioselective recognition and separation of racemic alcohols. *Dalton Trans.* **44**, 5692-5702 (2015).

69 Rajasekar, P. *et al.* Imido-P(v) trianion supported enantiopure neutral tetrahedral Pd(II) cages. *Chem. Commun.* **54**, 1873-1876 (2018).

70 Rajasekar, P. *et al.* Chiral separation of styrene oxides supported by enantiomeric tetrahedral neutral Pd(II) cages. *Inorg. Chem.* **58**, 15017-15020 (2019).

71 Hartlieb, K. J. *et al.* CD-MOF: A versatile separation medium. *J. Am. Chem. Soc.* **138**, 2292-2301 (2016).

72 Peng, Y. *et al.* Engineering chiral porous metal-organic frameworks for enantioselective adsorption and separation. *Nat. Commun.* **5**, 4406 (2014).

73 Qian, H.-L., Yang, C.-X. & Yan, X.-P. Bottom-up synthesis of chiral covalent organic frameworks and their bound capillaries for chiral separation. *Nat. Commun.* **7**, 12104 (2016).

74 Navarro-Sanchez, J. *et al.* Peptide metal-organic frameworks for enantioselective separation of chiral drugs. *J. Am. Chem. Soc.* **139**, 4294-4297 (2017).

75 Zhao, J. *et al.* Chirality from substitution: enantiomer separation via a modified metal–organic framework. *J. Mater. Chem. A* **3**, 12145-12148 (2015).

76 Das, M. C. *et al.* Interplay of metalloligand and organic ligand to tune micropores within isostructural mixed-metal organic frameworks (M'MOFs) for their highly selective separation of chiral and achiral small molecules. *J. Am. Chem. Soc.* **134**, 8703-8710 (2012).

77 Zhang, W. Y., Lin, Y. J., Han, Y. F. & Jin, G. X. Facile separation of regioisomeric compounds by a heteronuclear organometallic capsule. *J. Am. Chem. Soc.* **138**, 10700-10707 (2016).

78 Li, G. *et al.* Self-assembly of a homochiral nanoscale metallacycle from a metallosalen complex for enantioselective separation. *Angew. Chem. Int. Ed.* **47**, 1245-1249 (2008).

79 Li, G., Yu, W. & Cui, Y. A homochiral nanotubular crystalline framework of metallomacrocycles for enantioselective recognition and separation. *J. Am. Chem. Soc.* **130**, 4582-4583 (2008).

80 Xuan, W., Zhang, M., Liu, Y., Chen, Z. & Cui, Y. A chiral quadruple-stranded helicate cage for enantioselective recognition and separation. *J. Am. Chem. Soc.* **134**, 6904-6907 (2012).

81 Janczak, J. *et al.* Trinuclear cage-like Zn^{II} macrocyclic complexes: enantiomeric recognition and gas adsorption properties. *Chem. Eur. J.* **22**, 598-609 (2016).

82 Garcia-Simon, C. *et al.* Sponge-like molecular cage for purification of fullerenes. *Nat. Commun.* **5**, 5557 (2014).

83 Fuertes-Espinosa, C. *et al.* A copper-based supramolecular nanocapsule that enables straightforward purification of Sc_3N-based endohedral metallofullerene soots. *Chem. Eur. J.* **23**, 3553-3557 (2017).

84 Fuertes-Espinosa, C. *et al.* Purification of uranium-based endohedral metallofullerenes (EMFs) by selective supramolecular encapsulation and release. *Angew. Chem. Int. Ed.* **57**, 11294-11299 (2018).

85 Fuertes-Espinosa, C. *et al.* Highly selective encapsulation and purification of U-based C_{78}-EMFs within a supramolecular nanocapsule. *Nanoscale* **11**, 23035-23041 (2019).

86 Zhang, X. *et al.* Fine-tuning apertures of metal-organic cages: encapsulation of carbon dioxide in solution and solid state. *J. Am. Chem. Soc.* **141**, 11621-11627 (2019).

87 Li, J. R. & Zhou, H. C. Bridging-ligand-substitution strategy for the preparation of metal-organic polyhedra. *Nat. Chem.* **2**, 893-898 (2010).

88 Prakash, M. J. *et al.* Edge-directed $[(M_2)_2L_4]$ tetragonal metal-organic polyhedra decorated using a square paddle-wheel secondary building unit. *Chem. Commun.* **46**, 2049-2051 (2010).

89 Bloch, E. D. *et al.* Hydrocarbon separations in a metal-organic framework with open iron(II) coordination sites. *Science* **335**, 1606-1610 (2012).

90 Yang, S. *et al.* Supramolecular binding and separation of hydrocarbons within a functionalized porous metal–organic framework. *Nat. Chem.* **7**, 121-129 (2015).

91 Assen, A. H. *et al.* Ultra-tuning of the rare-earth fcu-MOF aperture size for selective molecular exclusion of branched paraffins. *Angew. Chem. Int. Ed.* **54**, 14353-14358 (2015).

92 Zhai, Q.-G. *et al.* An ultra-tunable platform for molecular engineering of high-performance crystalline porous materials. *Nat. Commun.* **7**, 13645 (2016).

93 Chen, K.-J. *et al.* Benchmark C_2H_2/CO_2 and CO_2/C_2H_2 separation by two closely related hybrid ultramicroporous materials. *Chem* **1**, 753-765 (2016).

94 Chen, B. *et al.* A microporous metal-organic framework for gas-chromatographic separation of alkanes. *Angew. Chem. Int. Ed.* **45**, 1390-1393 (2006).

95 Herm, Z. R. *et al.* Separation of hexane isomers in a metal-organic framework with triangular channels. *Science* **340**, 960-964 (2013).

96 Jin, Z. *et al.* A novel microporous MOF with the capability of selective adsorption of xylenes. *Chem. Commun.* **46**, 8612-8614 (2010).

97 Barea, E., Montoro, C. & Navarro, J. A. Toxic gas removal - metal-organic frameworks for the capture and degradation of toxic gases and vapours. *Chem. Soc. Rev.* **43**, 5419-5430 (2014).

98 Bobbitt, N. S. *et al.* Metal-organic frameworks for the removal of toxic industrial chemicals and chemical warfare agents. *Chem. Soc. Rev.* **46**, 3357-3385 (2017).

99 Oh, H. & Hirscher, M. Quantum sieving for separation of hydrogen isotopes using MOFs. *Eur. J. Inorg. Chem.* **2016**, 4278-4289 (2016).

100 Banerjee, D. *et al.* Potential of metal-organic frameworks for separation of xenon and krypton. *Acc. Chem. Res.* **48**, 211-219 (2015).

101 Xie, W., Cui, D., Zhang, S.-R., Xu, Y.-H. & Jiang, D.-L. Iodine capture in porous organic polymers and metal–organic frameworks materials. *Mater. Horiz.* **6**, 1571-1595 (2019).

102 Gao, Y. *et al.* The construction of amorphous metal-organic cage-based solid for rapid dye adsorption and time-dependent dye separation from water. *Chem. Eng. J.* **357**, 129-139 (2019).

103 Cui, P. F., Lin, Y. J., Li, Z. H. & Jin, G. X. Dihydrogen bond interaction induced separation of hexane isomers by self-assembled carborane metallacycles. *J. Am. Chem. Soc.* **142**, 8532-8538 (2020).

104 Robeson, L. M. Correlation of separation factor versus permeability for polymeric membranes. *J. Membr. Sci.* **62**, 165-185 (1991).

105 Robeson, L. M. The upper bound revisited. *J. Membr. Sci.* **320**, 390-400 (2008).

106 Yun, Y. N. *et al.* Defect-free mixed-matrix membranes with hydrophilic metal-organic polyhedra for efficient carbon dioxide separation. *Chem. Asian. J.* **13**, 631-635 (2018).

107 Furukawa, H., Kim, J., Ockwig, N. W., O'Keeffe, M. & Yaghi, O. M. Control of vertex geometry, structure dimensionality, functionality, and pore metrics in the reticular synthesis of crystalline metal-organic frameworks and polyhedra. *J. Am. Chem. Soc.* **130**, 11650-11661 (2008).

108 Fulong, C. R. P., Liu, J., Pastore, V. J., Lin, H. & Cook, T. R. Mixed-matrix materials using metal-organic polyhedra with enhanced compatibility for membrane gas separation. *Dalton Trans.* **47**, 7905-7915 (2018).

109 Ma, J. *et al.* Mixed-matrix membranes containing functionalized porous metal-organic polyhedrons for the effective separation of CO_2-CH_4 mixture. *Chem. Commun.* **51**, 4249-4251 (2015).

110 Perez, E. V., Balkus, K. J., Ferraris, J. P. & Musselman, I. H. Metal-organic polyhedra 18 mixed-matrix membranes for gas separation. *J. Membr. Sci.* **463**, 82-93 (2014).

111 Liu, X. *et al.* Molecular-scale hybrid membranes derived from metal-organic polyhedra for gas separation. *ACS Appl. Mater. Interfaces* **10**, 21381-21389 (2018).

112 Kitchin, M. *et al.* AIMs: a new strategy to control physical aging and gas transport in mixed-matrix membranes. *J. Mater. Chem. A* **3**, 15241-15247 (2015).

113 Zhao, C. *et al.* Hybrid membranes of metal-organic molecule nanocages for aromatic/aliphatic hydrocarbon separation by pervaporation. *Chem. Commun.* **50**, 13921-13923 (2014).

114 Zhao, C. *et al.* Functionalized metal-organic polyhedra hybrid membranes for aromatic hydrocarbons recovery. *AIChE J.* **62**, 3706-3716 (2016).

115 Andres, M. A. *et al.* Ultrathin films of porous metal-organic polyhedra for gas separation. *Chem. Eur. J.* **26**, 143-147 (2020).

116 Liu, J. *et al.* Self-healing hyper-cross-linked metal-organic polyhedra (HCMOPs) membranes with antimicrobial activity and highly selective separation properties. *J. Am. Chem. Soc.* **141**, 12064-12070 (2019).

117 Li, Z., Mao, Z., Zhou, W. & Chen, Z. Incorporation of homochiral metal-organic cage into ionic liquid based monolithic column for capillary electrochromatography. *Anal. Chim. Acta* **1094**, 160-167 (2020).

118 He, L. X. *et al.* Chiral metal-organic cages used as stationary phase for enantioseparations in capillary electrochromatography. *Electrophoresis* **41**, 104-111 (2020).

119 Xie, S. M. *et al.* Homochiral metal-organic cage for gas chromatographic separations. *Int J Environ Anal Chem* **90**, 9182-9188 (2018).

120 Bojdys, M. J. *et al.* Supramolecular engineering of intrinsic and extrinsic porosity in covalent organic cages. *J. Am. Chem. Soc.* **133**, 16566-16571 (2011).

121 Hasell, T. & Cooper, A. I. Porous organic cages: soluble, modular and molecular pores. *Nat. Rev. Mater.* **1** (2016).

122 Ma, L. *et al.* Coordination cages as permanently porous ionic liquids. *Nat. Chem.* **12**, 270-275 (2020).

123 Jie, K. *et al.* Transforming porous organic cages into porous ionic liquids via a supramolecular complexation strategy. *Angew. Chem. Int. Ed.* **59**, 2268-2272 (2020).

124 Zhang, J. *et al.* Porous liquids: a promising class of media for gas separation. *Angew. Chem. Int. Ed.* **54**, 932-936 (2015).

125 Giri, N. *et al.* Liquids with permanent porosity. *Nature* **527**, 216-220 (2015).

126 Mastalerz, M. Liquefied molecular holes. *Nature* **527**, 174-175 (2015).